

Experimental investigation and thermodynamic calculation of Ni–Al–La ternary system in nickel-rich region: A new intermetallic compound Ni₂AlLa

LIAO, Jinfa, WANG, Hang and CHEN, Tzu-Yu <<http://orcid.org/0000-0002-1868-5314>>

Available from Sheffield Hallam University Research Archive (SHURA) at:
<https://shura.shu.ac.uk/23551/>

This document is the Published Version [VoR]

Citation:



LIAO, Jinfa, WANG, Hang and CHEN, Tzu-Yu (2018). Experimental investigation and thermodynamic calculation of Ni–Al–La ternary system in nickel-rich region: A new intermetallic compound Ni₂AlLa. *Materials*, 11 (12), p. 2396. [Article]

Copyright and re-use policy

See <http://shura.shu.ac.uk/information.html>

Article

Experimental Investigation and Thermodynamic Calculation of Ni–Al–La Ternary System in Nickel-Rich Region: A New Intermetallic Compound Ni_2AlLa

Jinfa Liao ¹ , Hang Wang ^{1,*} and Tzu-Yu Chen ^{2,*} 

¹ School of Materials Science and Engineering/Institute of Engineering Research, Jiangxi University of Science and Technology, Ganzhou 341000, China; 6720170477@mail.jxust.edu.cn

² Materials and Engineering Research Institute, Faculty of Science, Technology and Arts, Sheffield Hallam University, City Campus, Howard Street, Sheffield S1 1WB, UK

* Correspondence: wanghang@jxust.edu.cn (H.W.); t.chen@shu.ac.uk (T.-Y.C.)

Received: 14 November 2018; Accepted: 26 November 2018; Published: 28 November 2018



Abstract: The phase equilibrium of the Ni–Al–La ternary system in a nickel-rich region was observed at 800 °C and 1000 °C using scanning electron microscopy backscattered electron imaging, energy dispersive X-ray spectrometry and X-ray diffractometry. The solubility of Al in the Ni_5La phase was remeasured at 800 °C and 1000 °C. Herein, we report a new ternary phase, termed Ni_2AlLa , confirmed at 800 °C. Its X-ray diffraction (XRD) pattern was indexed and space group determined using Total Pattern Solution (TOPAS), and the suitable lattice parameters were fitted using the Pawley method and selected-area electron diffraction. Ni_2AlLa crystallizes in the trigonal system with a space group $R\bar{3}$ (no. 146), $a = 4.1985 \text{ \AA}$ and $c = 13.6626 \text{ \AA}$. A self-consistent set of thermodynamic parameters for the Al–La and Ni–La binary systems and the Ni–Al–La ternary system includes a Ni_2AlLa ternary phase, which was optimized using the CALPHAD method. The calculated thermodynamic and phase-equilibria data for the binary and ternary systems are consistent with the literature and measured data.

Keywords: Ni–Al–La; CALPHAD; lanthanides; thermodynamic optimization; superalloys

1. Introduction

Nickel-based single-crystal superalloys are used extensively in the blades of power turbines in modern aero-engines because of their excellent high-temperature properties, such as high-temperature strength, excellent creep and fatigue resistance, good oxidation resistance and hot corrosion resistance [1–4]. However, as the aero-engine thrust-to-weight ratio increases, turbine engines face the challenge of higher temperatures, and a nickel-based single-crystal superalloy is required to improve their high-temperature oxidation resistance and high-temperature corrosion resistance. The excellent performance of nickel-based superalloys is attributed to the addition of elements, such as Al, Mo, Cr, W, V and Ti [1]. Among these, the addition of a small amount of the rare-earth element La can significantly improve high-temperature oxidation resistance, corrosion resistance [5,6] and manufacturing performance [7]. However, excessive addition leads to an increase in the tendency to form a topologically close-packed (TCP) phase and to deterioration in the alloy properties [8], therefore it is vital that the amount of La added is precisely controlled. Alloy design depends on the thermodynamic database [9,10] CALPHAD (CALculation of PHase Diagram) method [11–13] which can reduce the experimental time, shorten the development cycle and provide theoretical guidance for material design. In this study, we consider the rare-earth element La and use the CALPHAD method to

optimize the Ni–Al–La ternary system thermodynamically and to establish a nickel-based superalloy database [14] which contains the rare-earth element, La.

Limited experimental equilibrium information exists for the Ni–Al–La ternary system. In the 1980s, Abramyan [15] studied a small part of the phase-equilibrium information at 800 °C and 1000 °C in the nickel-rich corner, although no detailed experimental data were provided. Therefore, it is important and necessary to acquire phase-equilibrium information for the Ni–Al–La ternary system to obtain more accurate thermodynamic parameters and to provide effective and reasonable theoretical guidance for the design of nickel-based superalloys.

The purpose of this work was to investigate the phase equilibria relationship of the Ni–Al–La system in the nickel-rich region at 800 °C and 1000 °C by using scanning electron microscopy (SEM)-backscattered electron imaging (BSE), energy dispersive X-ray spectroscopy (EDS) and X-ray diffraction (XRD). Based on the experimental results of this study and previous literature data, a thermodynamic assessment of the Ni–Al–La system was conducted using the CALPHAD approach.

2. Literature Review

2.1. Al–La Binary System

Phase-equilibrium information on the Al–La binary system has been widely reported in the literature [16–19]. Four solid-solution phases (liquid, fcc, bcc, dhcp) and six intermetallic compounds (AlLa_3 , Al_2La , AlLa , Al_7La_3 , Al_3La , $\text{Al}_{11}\text{La}_3$) exist, including an allotropic transformation of the $\text{Al}_{11}\text{La}_3$ phase. La solubility in Al solid solution was reported by Drits et al. [20]. Thermodynamic optimization of the Al–La system has been conducted by various authors [21–25]; however, the latest experimental data [18] were not considered in previous optimization work [21]. An associate model and modified quasichemical model were applied to the liquid phase in the work of Zhou and Napolitano [24] and Jin [25], respectively, which is not applicable in the pan-nickel database. The calculated temperature of the peritectoid reaction $\text{Al}_7\text{La}_3 \rightarrow \text{Al}_3\text{La} + \text{Al}_2\text{La}$ was 1051 °C [23], which deviates substantially from the experimental value of 1190 °C [16]. The phase diagram and thermodynamic evaluation calculated by Yin et al. [22] are consistent with the literature data, however, the $\text{Al}_{11}\text{La}_3$ phase is not treated as $\beta\text{-Al}_{11}\text{La}_3$ and $\alpha\text{-Al}_{11}\text{La}_3$. Therefore, our work adds an allotropic transformation on this basis, and adjusts the parameters of the $\text{Al}_{11}\text{La}_3$ phase slightly. Furthermore, the solubility of La in the Al solid-solution is also considered.

2.2. Ni–La Binary System

The phase equilibria of the Ni–La binary system were measured by Zhang et al. [26], Qi et al. [27] and Buschow et al. [28]. In the assessment by Okamoto [29] and Pan et al. [30], there were four solution phases (liquid, fcc, bcc, dhcp) and nine intermediate phases (Ni_3La_7 , NiLa_3 , NiLa , Ni_3La_2 , $\text{Ni}_{16}\text{La}_7$, Ni_3La , $\alpha\text{-Ni}_7\text{La}_2$, $\beta\text{-Ni}_7\text{La}_2$, Ni_5La). Despite a reported new $\text{Ni}_{19}\text{La}_5$ phase [31–34], this phase has not been taken into account in the optimization work [35,36]. Recently An et al. [37] confirmed the formation of a $\text{Ni}_{19}\text{La}_5$ phase from a peritectoid reaction $\text{Liq.} + \text{Ni}_5\text{La} \rightarrow \text{Ni}_{19}\text{La}_5$, and this has also been considered in their optimization work. Therefore, we have used most of thermodynamic parameters from reference [37] in this work. Although the mutual solubilities of Ni and La in the terminal solution phases of the La (hcp, bcc, fcc) and Ni (fcc) are very low, the high-temperature oxidation resistance of a nickel-based superalloy can be improved by La solubility. Hence, the solubility of La (0.2 ± 0.05 at.%) measured by Dischinger et al. [35] was used in this assessment.

2.3. Ni–Al Binary System

The Ni–Al binary system has been assessed in our previous work [38] and is adjusted slightly based on Huang's thermodynamic parameters [39]. The Ni–Al phase diagram as shown in Figure 1, and thermodynamic parameters of the Ni–Al system have been adopted from previous work without changes.

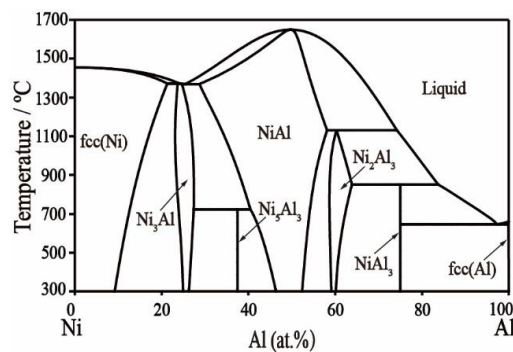


Figure 1. Calculated Ni–Al phase diagram.

2.4. Ni–Al–La Ternary System

The Ni–Al–La ternary system was assessed by Ferro et al. [40] and Raghavan [41]. Two isothermal sections at the nickel-rich corner were measured at 800 °C and 1000 °C by a hardness and X-ray diffraction method, however, detailed experimental data were lacking, and only phase-equilibrium information was obtained [15]. The author also reported that the solubility of Al in the Ni₅La phase increased with temperature and exceeded 20 at.%. Based on his paper, we found that the solubility of Al in Ni₅La is of the order of 23 at.% at 800 °C, and increases to 25 at.% at 1000 °C. A vertical section Al₉₀La–Al₉₀Ni was determined by Gödecke et al. using a metallographic observation and a DTA method [42], and a ternary eutectic reaction $\text{Liq} \rightarrow \text{Fcc} + \text{Al}_{11}\text{La}_3 + \text{Al}_3\text{Ni}$ at 625 °C was determined. Cordier et al. [43] and Takeshita et al. [44] reported the intermetallic compounds NiAlLa and Ni₄AlLa in the nickel-rich corner. The open-source first-principle-database Open Quantum Materials Database (OQMD) [45], Materials Project [46] and Aflow (Automatic flow) [47] provide the ternary intermetallic-compound and crystal-structure information using first-principles calculation. All ternary intermetallic compounds and their crystal structures in the nickel-rich region of the Ni–Al–La ternary system from the literature and the open-source first-principle databases are listed in Table 1.

The enthalpies of mixing of the ternary liquid at different sections were measured by Feufel et al. [48] with an adiabatic calorimeter. Sommer and Schmid [49,50] adopted the same method to study the heat of the liquid Ni–Al–La alloy, but the liquidus temperature values of the Ni–Al–La alloys obtained from C_p -measurements were very low in comparison to the melting temperatures of the alloy, which resulted in the C_p values of their work exceeding the actual value. Thus, their thermodynamic optimization procedure is not utilized in this work. Additionally, Pasturl et al. [51] and Borzone et al. [52] used isoperibol calorimetry and a high-temperature direct-reaction drop calorimeter, respectively, to determine the formation of Ni₄AlLa and NiAlLa ternary intermetallic compounds.

Table 1. Crystal structure of ternary compound in nickel-rich corner of Ni–Al–La ternary system from different sources.

Crystal System	Space Group	Structure Type	Lattice Constants (Å)			Source
			a	b	c	
Ni ₉ Al ₂ La	<i>Cmmm</i>	-	8.599	5.040	8.062	OQMD
	<i>F1</i>	-	5.048	8.599	8.035	Materials project
Ni ₄ AlLa	<i>P6/mmm</i>	CaCu ₅	5.069	5.069	4.074	[51]
NiAlLa	<i>Pnma</i>	-	7.199	4.203	16.085	[52]
Ni ₂ AlLa	<i>Fm-3m</i>	Cu ₂ MnAl	6.724	6.724	6.724	OQMD
	<i>P4/mmm</i>	-	4.640	4.640	3.1615	Aflow
	<i>P4/mmm</i>	-	3.117	3.117	6.793	Aflow
	<i>P4/mmm</i>	-	3.074	3.074	6.900	Aflow
	<i>P4/mmm</i>	-	3.126	3.126	6.919	Aflow
	<i>Cm</i>	-	4.001	7.189	5.641	Aflow
	<i>Fm-3m</i>	-	6.536	6.536	6.536	Aflow
	<i>Pmm2</i>	-	3.129	3.159	6.875	Aflow
	<i>F-43m</i>	-	6.591	6.591	6.591	Aflow
	<i>Cmmm</i>	-	6.574	6.596	3.141	Aflow
	<i>I-4m2</i>	-	4.012	4.012	8.892	Aflow

3. Materials and Methods

Four representative alloys, each weighing 15 g on an electronic balance with an accuracy of 0.0001 g, were prepared using high-purity nickel (99.99 wt.%), aluminum (99.999 wt.%) and lanthanum (99.9 wt.%) as starting materials. Mixed metals were transferred into a water-cooled copper-crucible arc furnace, vacuumed to 10^{-3} Pa and smelted in a high-purity argon (99.999%) atmosphere. Each sample was turned over and re-melted at least six times during the smelting process to ensure a homogeneous composition. The mass loss during arc smelting was less than 0.5 wt.%. The smelted sample was cut into two parts by a wire-cutting machine and sealed in quartz tubes which were evacuated and filled with high-purity argon gas for annealing at 800 °C and 1000 °C for 30 days and 15 days, respectively. Finally, the quartz tubes were quenched in cold water and broken.

The X-ray diffraction data for all alloys were obtained at room temperature using a Bruker SMART APEX II single-crystal X-ray diffractometer (Karlsruhe, Germany) with Cu $K\alpha$ -radiation in the 2θ scan range of 10–90°. The alloy phase distributions were observed by BSE imaging of the FEI MLA650F field-emission SEM (Hillsboro, OR, USA) after standard metallographic preparation, and the elemental composition of the phases was measured by equipped EDS. The crystallographic information of the intermetallic compound was indexed using Total Pattern Solution (TOPAS) [53] software (TOPAS-Academic 6) and Pawley fits were carried out to refine lattice parameters and confirm space groups of the phases recorded before structure solution was attempted [54]. To further support the structural information acquired from XRD, we ground the alloy to below 100- μ m thick and performed ion thinning (Gatan 691) and a FEI Tecnai G2 F20 (Hillsboro, OR, USA) for selected area electron diffraction (SAED).

4. Calculations

Pandat software [55] was used for thermodynamic calculations. The thermodynamic model for the Gibbs free energy G of the solution phases, including liquid, fcc, bcc and dhcp, is:

$$G_m^\varphi = \sum_{i=\text{Al,Ni,La}} \left(x_i {}^0G_i^\varphi \right) + RT \sum_{i=\text{Al,Ni,La}} \left(x_i \ln(x_i) \right) + {}^{\text{ex}}G_m^\varphi \quad (1)$$

where i represents elements Al, La and Ni; x is the composition; ${}^0G_i^\varphi$ is the Gibbs free energy for pure element i in the structure φ phase and is obtained from Dinsdale [56]; R is the gas constant; T is the temperature in K; and ${}^{\text{ex}}G_m^\varphi$ is the excess Gibbs free energy, which is described as:

$${}^{\text{ex}}G_m^\varphi = x_{\text{Al}}x_{\text{Ni}}L_{\text{Al,Ni}}^\varphi + x_{\text{Al}}x_{\text{La}}L_{\text{Al,La}}^\varphi + x_{\text{La}}x_{\text{Ni}}L_{\text{La,Ni}}^\varphi + x_{\text{Al}}x_{\text{Ni}}x_{\text{La}}L_{\text{Al,Ni,La}}^\varphi \quad (2)$$

where $L_{\text{Al,Ni}}^\varphi$, $L_{\text{Al,La}}^\varphi$ and $L_{\text{La,Ni}}^\varphi$ are the interaction parameters in the Al–Ni, Al–La and La–Ni binary systems and the $L_{\text{Al,Ni,La}}^\varphi$ corresponds to the interaction parameters of the Ni–Al–La ternary system. All parameters were obtained by optimizing the experimental data.

Thermodynamic models for most of the binary phases were taken from previous work [22,37,38] except for the Ni_5La phase. Because of the solubility of Al in the Ni_5La phase, the thermodynamic model for the Ni_5La phase was modified to:

$$G^{(\text{Al,Ni})_5\text{La}} = y_{\text{Al}}G_{\text{Al:La}} + y_{\text{Ni}}G_{\text{La:Ni}} + 5RT(y_{\text{Al}} \ln(y_{\text{Al}}) + y_{\text{Ni}} \ln(y_{\text{Ni}})) + y_{\text{Al}}y_{\text{Ni}}L_{\text{La:Al,Ni}} \quad (3)$$

where y_{Al} and y_{Ni} are the site fractions of Al and Ni in the first sublattice; $G_{\text{Al:La}}$ and $G_{\text{La:Ni}}$ are Gibbs free energies for end-members and $L_{\text{La:Al,Ni}}$ is the interaction term between the two sublattices to be optimized.

Ternary intermetallic $\text{Ni}_m\text{Al}_n\text{La}_1$ phases were treated as stoichiometric compounds, and the Gibbs free energy was expressed as:

$$G_{\text{Al:Ni:La}}^{\text{Ni}_2\text{AlLa}} = nx_{\text{Al}} G_{\text{Al}}^{\text{fcc}} + lx_{\text{La}} G_{\text{La}}^{\text{dhcp}} + mx_{\text{Ni}} G_{\text{Ni}}^{\text{fcc}} + A + BT \quad (4)$$

where A and B are the thermodynamic parameters to be optimized.

5. Results and Discussion

5.1. Microstructure and Phase Equilibria

BSE images of the Ni–Al–La ternary alloys are shown in Figure 2, and EDS results in Table 2. All components were expressed in atomic percentage. #1 alloy exhibits a three-phase equilibrium at 800 °C as shown in Figure 2a. The dark area indicates a NiAl phase and the light-grey area is an unknown phase. A few bright-phase regions contain very fine precipitates and irregular stripes, which are likely to be the liquid phase prior to alloy removal from the furnace, and fine precipitates and irregular stripes formed during solidification. The unknown phase is a new phase consisting of 52.63Ni–24.02Al–23.36La based on the EDS result. This phase indicates a Ni_2AlLa ternary phase that has not been measured experimentally, but only calculated using an ab initio method in the Ni–Al–La ternary system of the OQMD and Aflow database. Figure 2b shows the two-phase microstructure (Ni_2AlLa + liquid) of the #2 alloy annealed at 800 °C for 30 days. The light-grey region is an unknown phase and is likely the Ni_2AlLa phase from the EDS result (53.47Ni–23.74Al–22.79). The remaining stripes are precipitated by liquid during cooling. Figure 2c shows the three-phase region of #3 alloy at 800 °C. The dark area indicates a NiAl phase, where the dark-grey area is the $(\text{Ni}, \text{Al})_5\text{La}$ phase and the light-grey area is an unknown phase. This light-grey component is likely to be 51.83Ni–24.30Al–23.86La from the EDS result, and it is suggested that it is the same phase, Ni_2AlLa , observed in the #1 and #2 alloys. Figure 2d presents the two-phase equilibrium microstructure in the #4 alloy annealed at 800 °C for 30 days. The dark area is the NiAl phase, and the dark-grey area is the $(\text{Ni}, \text{Al})_5\text{La}$ phase. Figure 2e shows the presence of a two-phase region (NiAl + liquid) for the #1 alloy annealed at 1000 °C for 15 days. The dark region is the NiAl phase and an irregular stripe is formed during the cooling of the liquid phase. Figure 2f shows the BSE image of the #2 alloy annealed at 1000 °C for 15 days. All stripes were formed during liquid solidification, so this is a single-phase region. Figure 2g,h represent the BSE images of #3 and #4 alloys, respectively, annealed at 1000 °C for 15 days, which represent the three-phase region (NiAl + $(\text{Ni}, \text{Al})_5\text{La}$ + liquid). The dark region is the NiAl phase, the dark-grey area is the $(\text{Ni}, \text{Al})_5\text{La}$ phase, the bright region contains very fine precipitates, and the irregular stripes were the liquid phase prior to the alloy removal from the furnace.

$(\text{Ni}, \text{Al})_5\text{La}$ is a solid solution, based on the Ni_5La binary phase. The $(\text{Ni}, \text{Al})_5\text{La}$ phase exists in the #3 and #4 alloys. According to the corresponding EDS results, the maximum solubility of Al in Ni_5La is 23.53 at.% at 800 °C, which is consistent with the experimental value (23.53 at.%) reported by Abramyan in 1979 [15]. When the temperature reaches 1000 °C, the maximum solubility of Al in Ni_5La is in the order of 19.78 at.%, which is much less than the 25 at.% reported by Abramyan. Because of the unreliable experimentation and the lack of detailed experimental data in Abramyan's results [15], the value of solid solution of Al in Ni_5La is not convincing. Thus, the maximum solubility of Al in Ni_5La from our present work is more reliable as the key experiment was done. The reason the solubility of Al in Ni_5La at 1000 °C is less than that at 800 °C is mainly because with a temperature increase to 1000 °C, the liquid is more stable, which reduces the solubility of Al in the Ni_5La phase.

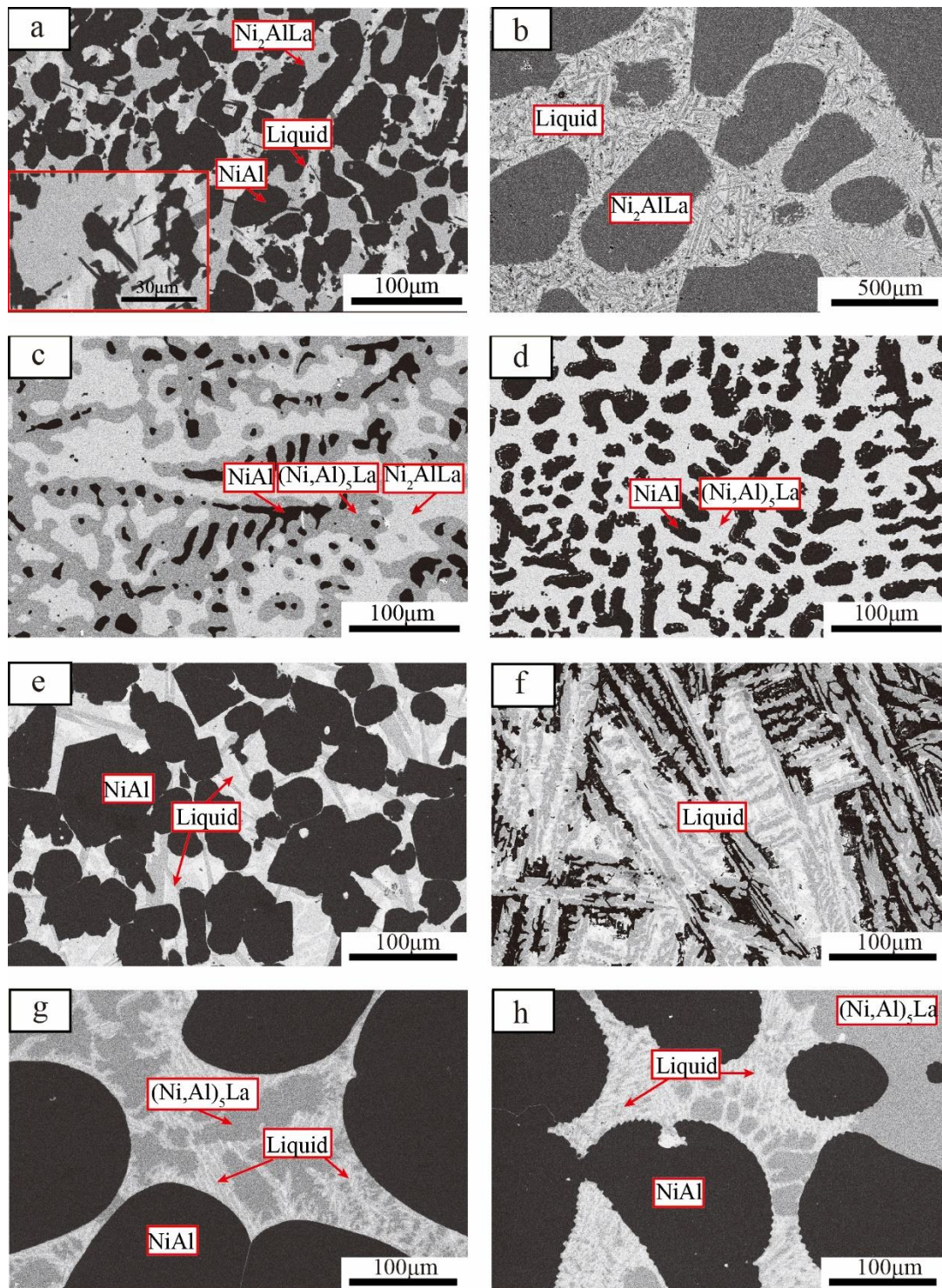


Figure 2. BSE images of ternary alloys annealed at 800 °C for 30 days: (a) #1 alloy, (b) #2 alloy, (c) #3 alloy, (d) #4 alloy. BSE images of ternary alloys annealed at 1000 °C for 15 days: (e) #1 alloy, (f) #2 alloy, (g) #3 alloy, (h) #4 alloy.

Table 2. Heat-treatment conditions and equilibrium composition of the determined Ni–Al–La ternary system.

Temperature	Alloys (at.%)	Annealed Time	Phase by XRD	Phase	Composition (at.%)		
				by SEM and EDS	Ni	Al	La
800 °C	Ni ₅₀ Al ₃₅ La ₁₅ (#1)	30 days	NiAl + Ni ₂ AlLa	NiAl	49.68	50.28	0.05
				Ni ₂ AlLa	53.63	23.02	23.36
				Liquid	22.87	43.30	33.83
	Ni ₅₀ Al ₁₈ La ₃₂ (#2)	30 days	Ni ₂ AlLa	Ni ₂ AlLa	53.47	23.74	22.79
				Liquid	50.04	6.61	43.38
	Ni ₅₇ Al ₂₃ La ₂₀ (#3)	30 days	Ni ₂ AlLa + Ni ₅ La	NiAl	50.48	49.05	0.47
				Ni ₂ AlLa	51.83	24.30	23.86
				Ni ₅ La	60.77	23.53	15.37
1000 °C	Ni ₆₀ Al ₃₀ La ₁₀ (#4)	30 days	NiAl + Ni ₅ La	NiAl	52.33	47.50	0.17
				Ni ₅ La	63.35	21.71	14.94
	Ni ₅₀ Al ₃₅ La ₁₅ (#1)	15 days	NiAl	NiAl	51.35	48.65	0.00
				Liquid	51.05	20.38	28.57
	Ni ₅₀ Al ₁₈ La ₃₂ (#2)	15 days		Liquid	57.03	10.72	27.85
	Ni ₅₇ Al ₂₃ La ₂₀ (#3)	15 days	NiAl + Ni ₅ La	NiAl	47.18	52.66	0.15
				Ni ₅ La	65.09	19.78	15.13
				Liquid	55.29	17.89	26.82
	Ni ₅₇ Al ₂₃ La ₂₀ (#4)	15 days	NiAl + Ni ₅ La	NiAl	46.74	53.26	0.00
				Ni ₅ La	66.95	17.95	15.09
				Liquid	55.29	17.75	26.96

5.2. Phase Determination

Figure 3 shows the XRD patterns obtained from #1 to #4 alloys annealed at 800 °C for 30 days and 1000 °C for 15 days. The #1 alloy exists in the three-phase region (NiAl + Ni₂AlLa + liquid). A NiAl phase was identified, and the remaining peaks result from the Ni₂AlLa phase and the liquid phase during cooling. The #2 alloy exists in the two-phase region (Ni₂AlLa + liquid) at 800 °C. Its corresponding XRD pattern is shown in Figure 3a. All peaks result from the Ni₂AlLa phase and the liquid phase during cooling. The three-phase region, NiAl + (Ni,Al)₅La + Ni₂AlLa, exists in the #3 alloy that was annealed at 800 °C. It contains two phases in the XRD pattern Figure 3a, (Ni,Al)₅La phase labelled with a triangle and possibly a new Ni₂AlLa phase. The NiAl phase was not observed due to the small amount. The potential characteristic peaks of the Ni₂AlLa phase in the #3 alloy annealed at 800 °C (marked with stars) were also found in the XRD pattern of the #1 and #2 alloys annealed at 800 °C. The #4 alloy is a two-phase region, and consists of the NiAl + (Ni,Al)₅La phase; all phases were confirmed. All alloy phases in the #1 to #4 alloys that were annealed at 1000 °C for 15 days have been identified as shown in Figure 3b, except the liquid phase. The unknown remaining peaks result from the liquid phase, because liquid-phase solidification is a complex phase-transition process.

A new phase, termed Ni₂AlLa, with a stoichiometric ratio of 2:1:1 (Ni:Al:La) was determined for the first time. It was observed in SEM-BSE, as shown in Figure 2 in the #1, #2 and #3 alloys annealed at 800 °C, as well as in the XRD presented in Figure 3a. Potential characteristic peaks of the Ni₂AlLa phase are indicated with stars. The crystal structure of the Ni₂AlLa phase was calculated by the ab initio method in the Ni–Al–La ternary system of the OQMD and Aflow database, and the calculated structures are listed in Table 1. The XRD pattern of the Ni₂AlLa phase calculated by the OQMD and Aflow database match our experimental measurements, so the crystal structure solution of the Ni₂AlLa phase was attempted. TOPAS was used to index the potential characteristic peaks of the Ni₂AlLa phase for possible lattice constants and space group. The suitable cell parameters and space groups were fitted using the whole powder pattern decomposition (WPPD) Pawley method. After satisfying Pawley fits of various candidates were achieved, we narrowed down to two different crystal structures for the new Ni₂AlLa intermetallic compound. Selective candidate cells are listed in Table 3. To confirm the crystal information from the XRD pattern is challenging at this stage due to the poor quality of the experimental XRD pattern. Furthermore, a great peak selection, which is essential for indexing, is hard

to perform due to the peaks overlapping from multiple-phase components. To further confirm the crystal information of this phase, SAED using TEM of the #3 alloy annealed at 800 °C was carried out.

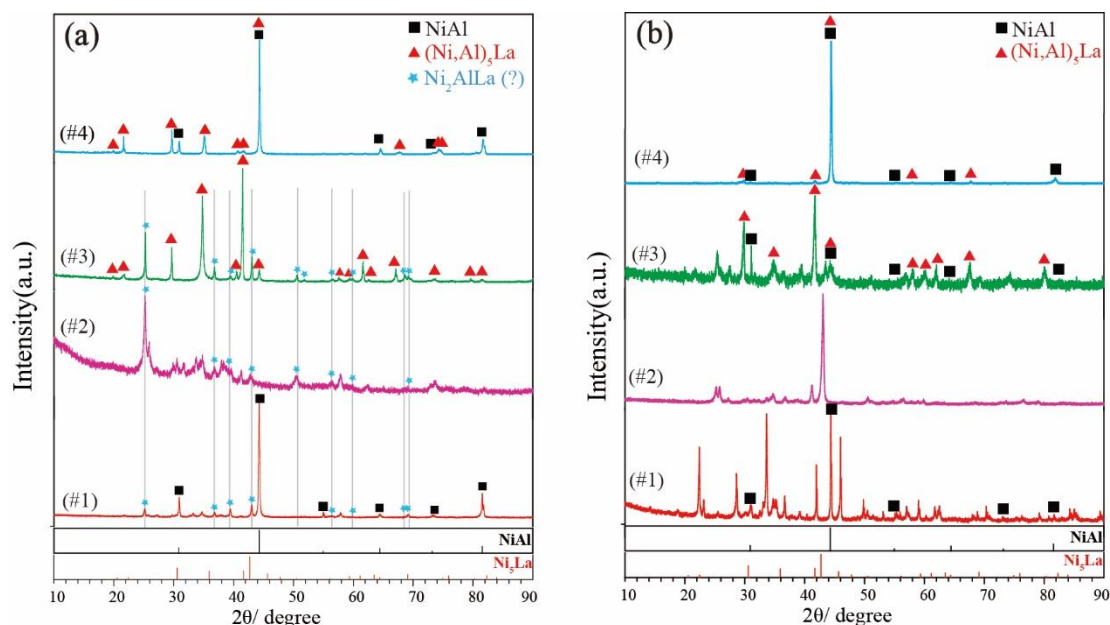


Figure 3. XRD patterns from: (a) Ni₅₀Al₃₅La₁₅ (#1), Ni₅₀Al₁₈La₃₂ (#2), Ni₅₇Al₂₃La₂₀ (#3) and Ni₆₀Al₃₀La₁₀ (#4) alloy annealed at 800 °C for 30 days; and (b) Ni₅₀Al₃₅La₁₅ (#1), Ni₅₀Al₁₈La₃₂ (#2), Ni₅₇Al₂₃La₂₀ (#3) and Ni₆₀Al₃₀La₁₀ (#4) alloy annealed at 1000 °C for 15 days.

Table 3. Possible crystal structure of the Ni₂AlLa intermetallic compound.

Crystal System	Space Group	Lattice Constants (Å)		
		a	b	c
Hexagonal/Trigonal	<i>P3c1</i>	10.740	10.740	3.367
	<i>R3</i>	4.189	4.189	14.663
	<i>P31c</i>	8.138	8.138	3.396
Orthorhombic	<i>F222</i>	9.739	10.130	2.195
	<i>C222</i>	3.263	2.733	7.021

Figure 4 presents the crystal morphology and SAED patterns of the #3 alloy annealed at 800 °C for 30 days, and indicates that a three-phase region, NiAl + (Ni,Al)₅La and Ni₂AlLa phase, existed. The calibration results of the SAED of the NiAl and Ni₅La phase are shown in Figure 4b,c. Figure 4b shows the diffraction spot of the NiAl phase on the [111] zone axis, and the diffraction spot of the (Ni,Al)₅La phase on the $\bar{1}\bar{1}1$ zone axis is exhibited in Figure 4c. For the Ni₂AlLa new phase, the SAED images of five different crystal zone axes were taken as shown in Figure 4e,f. The orthorhombic and hexagonal/trigonal cell choices obtained using TOPAS (Table 3) were used to calibrate the SAED image of the five different zone axes. It is impossible to calibrate any one of the SAED images using any of the two sets of lattice parameters of the orthorhombic system. Furthermore, the crystal structure of the Ni₂AlLa ternary phase calculated by the OQMD and Aflow database cannot calibrate any of the electron diffraction images. All electron-diffraction images were indexed and showed high agreement with the cell in the trigonal system *R3* space group, with the indexing result presented in Figure 4e,f. Based on the EDS, XRD and SAED results, a new Ni₂AlLa phase has been confirmed. The crystal structure of the Ni₂AlLa intermetallic compound was trigonal, with a space group *R3* (no. 146) and *a* = 4.185 Å, *c* = 13.6626 Å. The assignment of each reflection of the Ni₂AlLa phase with indices *hkl* based on the indexing result is shown in Figure 5.

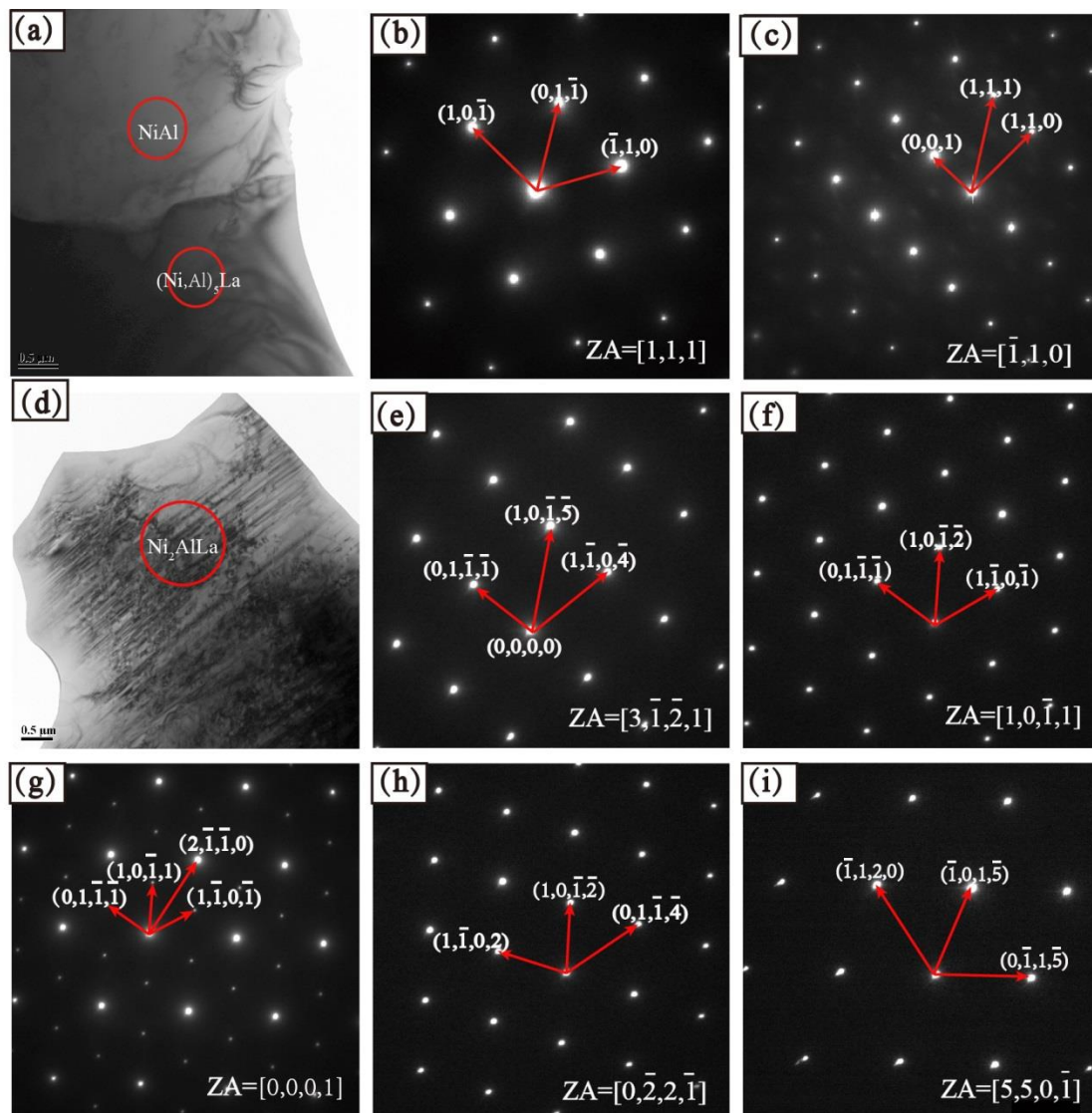


Figure 4. Crystal morphology and SAED patterns of #3 alloy annealed at 800 °C for 30 days. (a) crystal morphology of NiAl and (Ni, Al)₅La phase, (b) SAED image of NiAl phase with zone axis of [111], (c) SAED image of (Ni,Al)₅La phase with zone axis of $\bar{1}11$, (d) crystal morphology of Ni₂AlLa phase, (e) SAED image of Ni₂AlLa phase with zone axis of $3\bar{1}21$, (f) SAED image of Ni₂AlLa phase with zone axis of $10\bar{1}1$, (g) SAED image of Ni₂AlLa phase with zone axis of 0001 , (h) SAED image of Ni₂AlLa phase with zone axis of $02\bar{2}1$, (i) SAED image of Ni₂AlLa phase with zone axis of $550\bar{1}$.

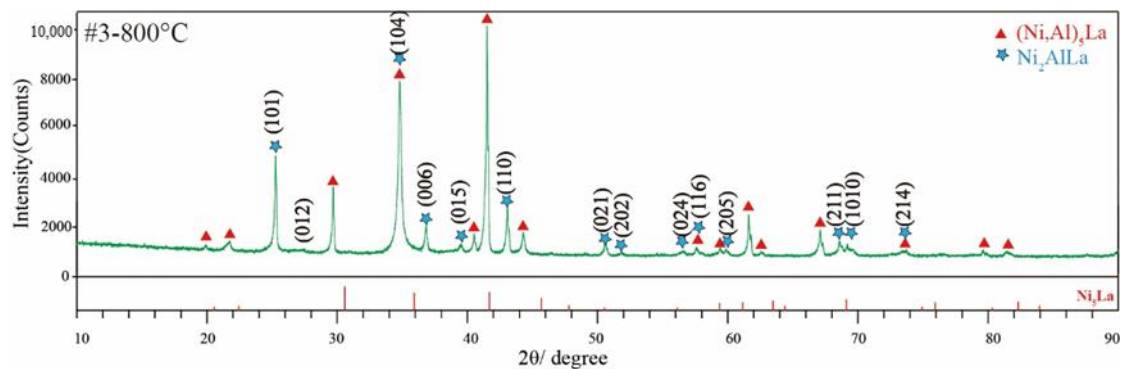


Figure 5. XRD pattern of #3 alloy annealed at 800 °C for 30 days.

5.3. Thermodynamic Calculation

Table 4 lists the optimized thermodynamic parameters for the Ni–Al binary system using the phase diagram as calculated in Figure 1. The phase diagram was calculated for the Ni–La binary system and is shown in Figure 6a. The solubility of La in the fcc Ni solution has been added, which fits the literature data [35] as shown in Figure 6b. The invariant reactions have not been affected, except the eutectic reaction $\text{Liq} \rightarrow \text{fcc-Ni} + \text{Ni}_7\text{La}_2$. The temperature (1272 °C) of this eutectic reaction increases by less than 4 °C compared with the reference [41] and is closer to the experimental data (1275 °C) [28]. The calculated phase diagram of the Al–La binary system is shown in Figure 7a. The solubility of La in the fcc-Al phase is also considered to be ~0.01 at.%, which is consistent with the experimental data [20] in Figure 7b. The $\text{Al}_{11}\text{La}_3$ phase is divided into two phases, $\alpha\text{-Al}_{11}\text{La}_3$ and $\beta\text{-Al}_{11}\text{La}_3$, according to their crystal structure stable at low and high temperature, respectively. The transformation temperature between the two $\text{Al}_{11}\text{La}_3$ phases is 915 °C, which is the same as that reported in the literature [16]. The temperature of the eutectic reaction $\text{Liq} \rightarrow \text{Fcc} + \alpha\text{-Al}_{11}\text{La}_3$ is calculated to be 631 °C, which is consistent with the 634 °C reported by Kononenko and Golubev [18]. Other invariant reactions remain unchanged. Overall, the calculated phase diagram in this work reproduces the literature data well.

Table 4. Optimized thermodynamic parameters of the Ni–Al–La ternary system.

Phase	Models	Parameters	Source
Liquid	(Al,Ni,La)	${}^0L_{\text{Al,Ni,La}}^{\text{Liq}} = 51,547 - 20T$	This work
		${}^1L_{\text{Al,Ni,La}}^{\text{Liq}} = 76,000 - 90T$	This work
		${}^2L_{\text{Al,Ni,La}}^{\text{Liq}} = 0$	This work
fcc	(Al,Ni,La)	${}^0L_{\text{Al,La}}^{\text{Fcc}} = -63,500 - 10T$	This work
		${}^1L_{\text{Al,La}}^{\text{Fcc}} = -80,000$	This work
		${}^0L_{\text{Ni,La}}^{\text{Fcc}} = -2000$	This work
		${}^1L_{\text{Ni,La}}^{\text{Fcc}} = -58,800$	This work
bcc	(Al,Ni,La)	${}^0L_{\text{Al,La}}^{\text{Bcc}} = -68,800$	This work
$\alpha\text{-Al}_{11}\text{La}_3$	$(\text{Al})_{11}(\text{La})_3$	${}^0G_{\text{Al:La}}^{\alpha\text{-Al}_{11}\text{La}_3} = -740,070.1 + 83.031T + 3 {}^0G_{\text{La}}^{\text{dhcp}} + 11 {}^0G_{\text{Al}}^{\text{fcc}}$	This work
$\beta\text{-Al}_{11}\text{La}_3$	$(\text{Al})_{11}(\text{La})_3$	${}^0G_{\text{Al:La}}^{\beta\text{-Al}_{11}\text{La}_3} = -738,882.1 + 82.031T + 3 {}^0G_{\text{La}}^{\text{dhcp}} + 11 {}^0G_{\text{Al}}^{\text{fcc}}$	This work
Ni_5La	$(\text{La})(\text{Al,Ni})_5$	${}^0G_{\text{La:Ni}}^{\text{Ni}_5\text{La}} = -168,451.2983 + 29.256T$	Ref [38]
		${}^0G_{\text{La:Al}}^{\text{Ni}_5\text{La}} = -8550 + 50T + {}^0G_{\text{La}}^{\text{dhcp}} + 5 {}^0G_{\text{Al}}^{\text{fcc}}$	This work
		${}^0L_{\text{La:Ni}}^{\text{Ni}_5\text{La}} = -939,000 + 50T$	This work
Ni_2AlLa	$(\text{Ni})_2(\text{Al})(\text{La})$	${}^0G_{\text{Al:Ni:La}}^{\text{Ni}_2\text{AlLa}} = -205,500 + 0.5T + G_{\text{Al}}^{\text{fcc}} + {}^0G_{\text{La}}^{\text{dhcp}} + 2 {}^0G_{\text{Ni}}^{\text{fcc}}$	This work

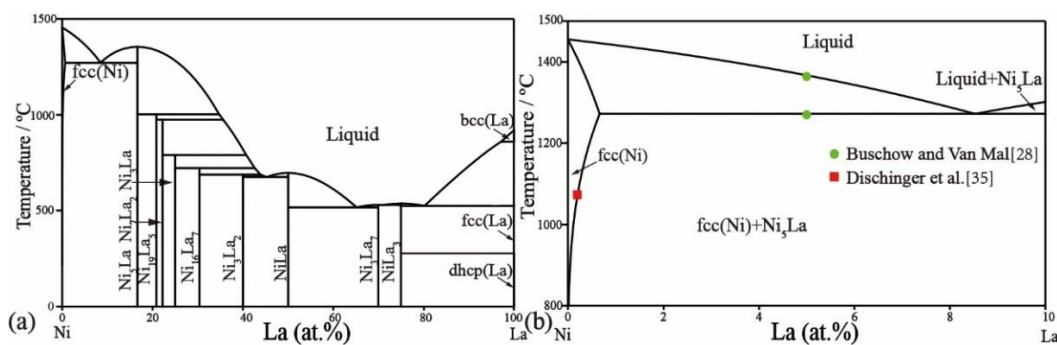


Figure 6. Calculated Ni–La phase diagram. (a) Full composition range, (b) magnified Ni-rich corner showing solubility of La in fcc(Ni).

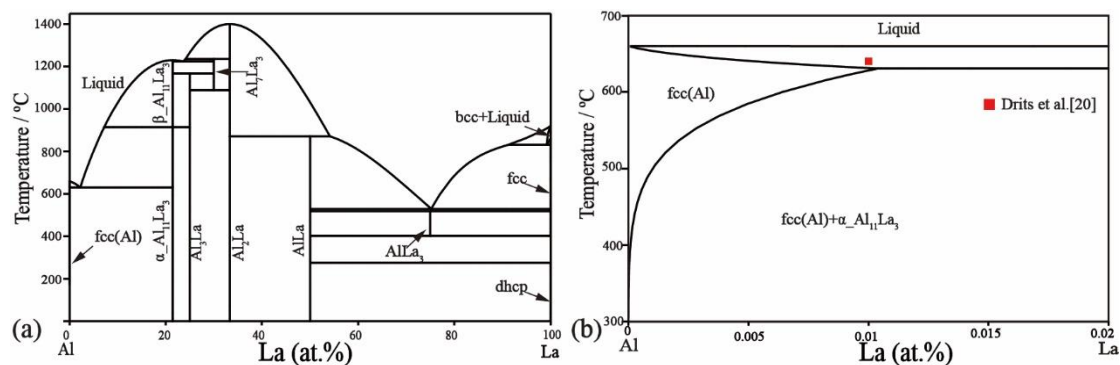


Figure 7. Calculated Al–La phase diagram. (a) Full composition range, (b) magnified Ni-rich corner showing solubility of La in fcc(Al).

The thermodynamic parameters of the Ni–Al–La ternary system optimized based on our experimental data and experimental information from the literature, are listed in Table 4. The calculated isothermal sections at 800 °C and 1000 °C are shown in Figures 8 and 9, where the red marks indicate the current experimental data. The phase-equilibrium information calculated for the isothermal sections shows high agreement with current experimental data. The calculated solubility of Al in the Ni_5La phase is 22.82 at.% and 19.72 at.% at 800 °C and 1000 °C, respectively, which is consistent with our current EDS results. The calculated phase equilibrium of the vertical section at Al_{90}La – Al_{90}Ni , as shown in Figure 10, matches the experimental literature data [42]. The eutectic reaction $\text{Liq} \rightarrow \text{Fcc} + \text{Al}_{11}\text{La}_3 + \text{Al}_3\text{Ni}$ temperature calculated in our work is 1 °C higher than the experimental value of 625 °C [42]. In general, the calculated phase-equilibrium information is consistent with both the previous literature and current experimental information. The calculated liquid-phase mixing of the different cross sections of the Ni–Al–La ternary is shown in Figure 11 compared with Reference [49], and it is clear that our results match those in the literature.

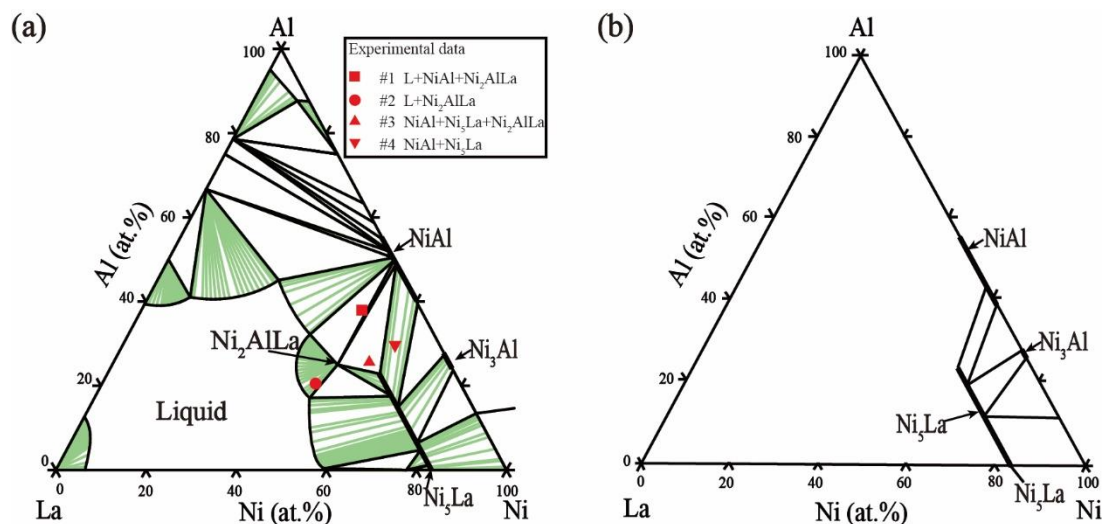


Figure 8. Isothermal section of the Ni–Al–La ternary system at 800 °C. (a) Our calculated isothermal section compared with our experimental results, (b) literature data [15].

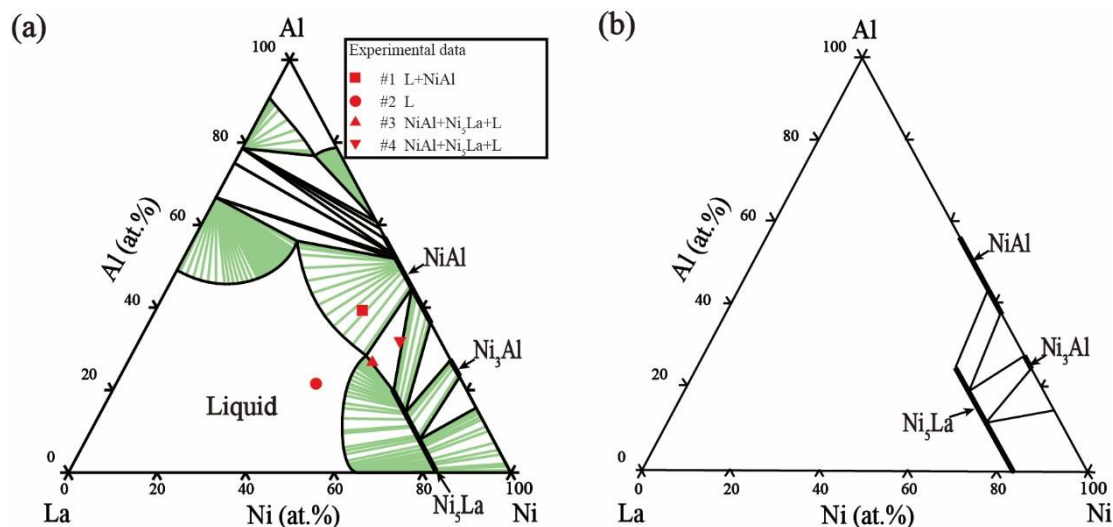


Figure 9. Isothermal section of the Ni–Al–La ternary system at 1000 °C. (a) Our calculated isothermal section compared with the experimental results, (b) literature data [15].

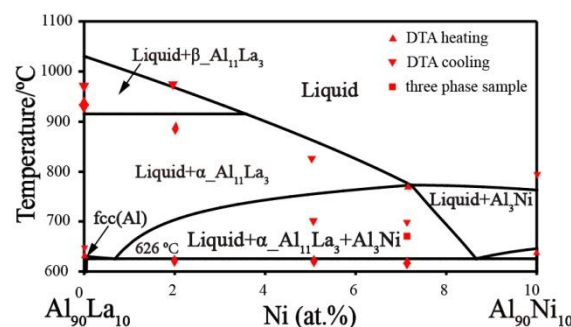


Figure 10. Calculated vertical section of Al₉₀La–Al₉₀Ni compared with the experimental data [42].

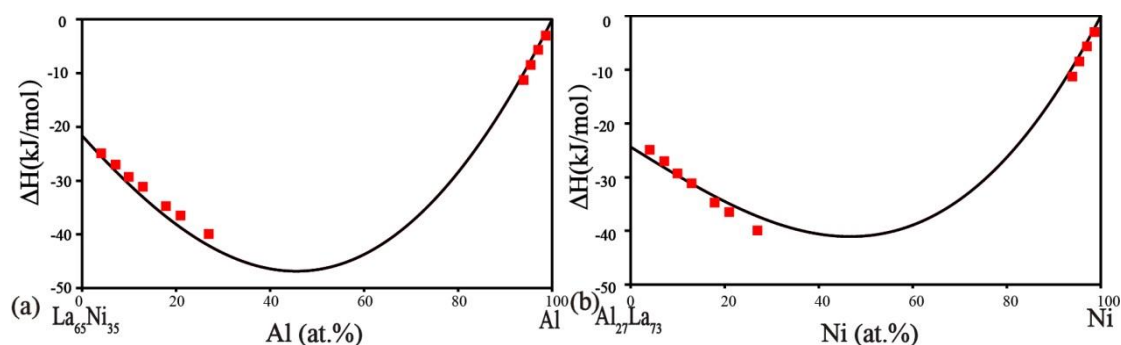


Figure 11. Calculated mixing enthalpies of the Ni–Al–La ternary system at 800 °C compared with experimental data [49], (a) (La₆₅Ni₃₅)_{1-x}Al_x section; (b) (Al₂₇La₇₃)_{1-x}Ni_x section.

6. Conclusions

1. The nickel-rich-region isothermal sections of the Ni–Al–La ternary system were updated at 800 °C and 1000 °C. The maximum solubility of Al in Ni₃La was in the order of 23.53 at.% at 800 °C. When the temperature increased to 1000 °C, the maximum solubility of Al in Ni₃La was 19.84 at.%.
2. A new phase, termed Ni₂AlLa, has been discovered experimentally and confirmed for the first time. The structural information of the new ternary intermetallic compound Ni₂AlLa was

determined. The investigated compound crystallizes in the trigonal system, space group $R\bar{3}$ (no. 146) with $a = 4.1985 \text{ \AA}$, $c = 13.6626 \text{ \AA}$.

3. Based on the current experimental data and experimental information reported in the literature, a thermodynamic optimization of the Ni–Al–La ternary system was carried out using the CALPHAD method. The solubility of La in the fcc (Ni) and fcc (Al) and an allotropic transformation of the $\text{Al}_{11}\text{La}_3$ phase were considered, and the Al–La and Ni–La binary systems were re-optimized. All optimized results and experimental information reflect good consistency. This work can be used as part of a thermodynamic database of multicomponent nickel-based alloys.

Author Contributions: H.W. put forward research scheme and the design concept, revised the draft and determined the final manuscript. T.-Y.C. analyzed the XRD data, revised and determined the final manuscript. J.L. carried out the main experiments and analyzed the data and wrote the main draft of the paper. All authors contributed to the discussion of the results and commented on the manuscript.

Funding: This research was funded by the National Natural Science Foundation of China, grant number 51761014, 51401095, and the Jiangxi Provincial Department of Science and Technology, China, grant number 20171BAB216004.

Acknowledgments: We thank Zheng and Zhang from ZKKF (Beijing) for help with the TEM support.

Conflicts of Interest: The authors declare no conflict of interest.

References

1. Reed, R.C. *The Superalloys: Fundamentals and Applications*; Cambridge University Press: Cambridge, UK, 2006.
2. Caron, P.; Lavigne, O. Recent studies at onera on superalloys for single crystal turbine blades. *Onera Aerosp. Lab. J.* **2011**, *3*, 1–14.
3. Kang, F.W.; Zhang, G.Q.; Sun, J.F.; Li, Z. Hot deformation behavior of a spray formed superalloy. *J. Mater. Process. Technol.* **2008**, *204*, 147–150. [[CrossRef](#)]
4. Pollock, T.M.; Tin, S. Nickel-based superalloys for advanced turbine engines: Chemistry, microstructure and properties. *J. Propuls. Power* **2006**, *22*, 361–374. [[CrossRef](#)]
5. Ford, D.A.; Fullagar, K.P.L.; Bhangu, H.K.; Thomas, M.C.; Burkholder, P.S.; Korinko, P.S.; Harris, K.; Wahl, J.B. Improved performance rhenium containing single crystal alloy turbine blades utilizing PPM levels of the highly reactive elements lanthanum and yttrium. *J. Eng. Gas Turbines Power* **1999**, *121*, 138–143. [[CrossRef](#)]
6. Song, X.; Wang, L.; Liu, Y. Effects of temperature and rare earth content on oxidation resistance of Ni-based superalloy. *Prog. Nat. Sci. Mater. Int.* **2011**, *21*, 227–235. [[CrossRef](#)]
7. Harris, K.; Wahl, J.B. Improved single crystal superalloys, CMSX-4(SLS)[La + Y] and CMSX-486. *Superalloys 2004*, *2004*, 45–52.
8. Pang, H.T.; Edmonds, I.M.; Jones, C.N.; Stone, H.J.; Rae, C.M.F. Effects of Y and La additions on the processing and properties of a second generation single crystal Nickel-base superalloy CMSX-4. *Superalloys 2012*, *2012*, 301–310.
9. Hoglund, Z.L.; Larsson, H.; Reed, R.C. Isolation of Optimal Compositions of Single Crystal Superalloys by Mapping of a Material's Genome. *Acta Mater.* **2015**, *90*, 330–343.
10. Reed, R.C.; Tao, T.; Warnken, N. Alloys-by-Design: Application to Nickel-Based Single Crystal Superalloys. *Acta Mater* **2009**, *57*, 5898–5913. [[CrossRef](#)]
11. Lukas, H.; Fries, S.G.; Sundman, B. *Computation Thermodynamics—The Calphad Method*; Cambridge University Press: Cambridge, UK, 2007.
12. Rettig, R.; Singer, R.F. Numerical modelling of precipitation of topologically close-packed phases in nickel-base superalloys. *Acta Mater.* **2011**, *59*, 317–327. [[CrossRef](#)]
13. Berthod, P.; Michon, S.; Martino, J.D. Thermodynamic calculations for studying high temperature oxidation of superalloys. *Calphad* **2003**, *27*, 279–288. [[CrossRef](#)]
14. Compu-Therm LLC, PanNickel Database. Available online: www.computherm.com (accessed on 27 November 2018).
15. Abramyan, A.K. Study of Interactions in the Nickel-rich Phases of the Aluminum-Lanthanum-Nickel system. *VINITI* **1979**, *3782*, 212–214.
16. Buschow, K.H.J. The lanthanum-aluminium system. *Philips. Res. Rep.* **1965**, *20*, 337–348.

17. Mesquita, A.H.G.D.; Buschow, K.H.J. The crystal structure of so-called α -LaAl₄ (La₃Al₁₁). *Acta Cryst.* **1967**, *22*, 497–501. [[CrossRef](#)]
18. Kononenko, V.I.; Golubev, S.V. On phase diagrams for binary systems of aluminium with La, Ce, Pr, Nd, Eu, Yb, Sc and Y. *Izvestiya Akademii Nauk SSSR Metall* **1990**, *19*, 197–199.
19. Ferro, R.; Saccone, A.; Delfino, S.; Cardinale, A.M.; Macciò, D. Inverse melting in binary systems: Morphology and microscopy of catatctic alloys. *Metall. Mater. Trans. B* **1996**, *27*, 979–986. [[CrossRef](#)]
20. Drits, M.E.; Kadaner, Z.S.; Nguyen, T.S. Solubility of Rare Earth Metals in Solid State Aluminium. *Izvestiya Akademii Nauk SSSR Metall* **1969**, *1*, 219–223.
21. Wang, J. Thermodynamic Optimization for Al-La System. *Calphad* **1994**, *18*, 269–272. [[CrossRef](#)]
22. Yin, F.; Su, X.; Li, Z.; Huang, M.; Shi, Y. A thermodynamic assessment of the La-Al system. *J. Alloys Compd.* **2000**, *1*, 169–172. [[CrossRef](#)]
23. Cacciamani, G.; Ferro, R. Thermodynamic modeling of Some aluminium-rare earth binary systems: Al-La, Al-Ce and Al-Nd. *Calphad* **2001**, *25*, 583–597. [[CrossRef](#)]
24. Zhou, S.H.; Napolitano, R.E. Phase equilibria and thermodynamic limits for partitionless crystallization in the Al-La binary system. *Acta Mater.* **2006**, *54*, 831–840. [[CrossRef](#)]
25. Jin, L.; Kang, Y.B.; Chartrand, P.; Fuerst, C.D. Thermodynamic evaluation and optimization of Al-La, Al-Ce, Al-Pr, Al-Nd and Al-Sm systems using the modified quasichemical model for liquids. *Calphad* **2011**, *35*, 30–41. [[CrossRef](#)]
26. Zhang, D.; Tang, J.; Gschneidner, K.A. A redetermination of the LaNi phase diagram from LaNi to LaNi₅ (50–83.3 at.% Ni). *J. Less-Common Met.* **1991**, *169*, 467–480.
27. Qi, G.J.; Li, Z.Q.; Yazawa, A.; Itagaki, K. High-temperature phase-relations in Ni-La, Ni-Ce, Ni-Pr, Ni-Nd binary and ternary alloy systems. *Mater. Trans. JIM* **1989**, *30*, 583–593. [[CrossRef](#)]
28. Buschow, K.H.; Mal, H.H.V. Phase relations and hydrogen absorption in the lanthanum-nickel system. *J. Less-Common Met.* **1972**, *29*, 203–210. [[CrossRef](#)]
29. Okamoto, H. La-Ni (Lanthanum-Nickel). *J. Phase Equilib.* **1991**, *12*, 615–616. [[CrossRef](#)]
30. Pan, Y.Y.; Nash, P. La-Ni (lanthanum-nickel). *J. Phase Equilib.* **2002**, *23*, 287–288.
31. Yamamoto, T.; Inui, H.; Yamaguchi, M.; Sato, K.; Fujitani, S.; Yonezu, I. Microstructures and hydrogen absorption/desorption properties of La-Ni alloys in the composition range of La 77.8~83.2 at.% Ni. *Acta Mater.* **1997**, *45*, 5213–5221. [[CrossRef](#)]
32. Férey, A.; Cuevas, F.; Latroche, M.; Knosp, B.; Bernard, P. Elaboration and characterization of magnesium-substituted La₅Ni₁₉ hydride forming alloys as active materials for negative electrode in Ni-MH battery. *Electrochim. Acta* **2009**, *54*, 1710–1714. [[CrossRef](#)]
33. Inui, H.; Yamamoto, T.; Zhang, D.; Yamaguchi, M. Microstructures and defect structures in intermetallic compounds in the La-Ni alloy system. *J. Alloys Compd.* **1999**, *293*, 140–145. [[CrossRef](#)]
34. Inui, H.; Yamamoto, T.; Zhang, D.; Yamaguchi, M. Characterization of stacking Faults on basal planes in intermetallic compounds La₅Ni₁₉ and La₂Ni₇. *Intermetallics* **2000**, *8*, 391–397.
35. Dischinger, J.; Schaller, H.J. Constitution and thermodynamics of Ni-La alloys. *J. Alloys Compd.* **2000**, *312*, 201–210. [[CrossRef](#)]
36. Liu, L.B.; Jin, Z.P. Thermodynamic reassessment of the La-Ni system. *Zeitschrift Metallkunde* **2000**, *91*, 739–743.
37. An, X.H.; Gu, Q.F.; Zhang, J.Y.; Chen, S.L.; Yu, X.B.; Li, Q. Experimental investigation and thermodynamic reassessment of La-Ni and LaNi₅-H systems. *Calphad* **2013**, *40*, 48–55. [[CrossRef](#)]
38. Huang, J.; Yang, B.; Chen, H. Thermodynamic optimisation of the Ni-Al-Y ternary System. *J. Phase Equilib. Diff.* **2015**, *36*, 357–365. [[CrossRef](#)]
39. Huang, W.; Chang, Y.A. A Thermodynamic Analysis of the Ni-Al System. *Intermetallics* **1998**, *6*, 487–498. [[CrossRef](#)]
40. Ferro, R.; Zanicchi, G.; Marazza, R.; Petzow, G. *Aluminium-Lanthanum-Nickel in Ternary Alloys: A Comprehensive Compendium of Evaluated Constitutional Data and Phase Diagrams*; Petzow, G., Effenberg, G., Eds.; Wiley-VHC: Weinheim, Germany, 1993; Volume 6, pp. 318–327.
41. Raghavan, V. Al-La-Ni (Aluminum-Lanthanum-Nickel). *J. Phase Equilib. Diff.* **2006**, *27*, 392.
42. Gödecke, T.; Sun, W.; Lück, R.; Lu, K. Metastable Al-Nd-Ni and Stable Al-La-Ni Phase Equilibria. *Zeitschrift Metallkunde* **2001**, *92*, 717–722.
43. Cordier, G.; Dörsam, G.; Kniep, R. New intermediate phases in the ternary systems rare earth-transition element-aluminium. *J. Magn. Magn. Mat.* **1988**, *76*, 653–654. [[CrossRef](#)]

44. Takeshita, T.; Malik, S.K.; Wallace, W.E. Hydrogen absorption in RNi_4Al (R = Rare Earth) ternary compounds. *J. Solid State, Chem.* **1978**, *23*, 271–274. [[CrossRef](#)]
45. Kirklin, S.; Saal, J.E.; Meredig, B.; Thompson, A.; Doak, J.W.; Aykol, M.; Rühl, S.; Wolverton, C. The Open Quantum Materials Database (OQMD): Assessing the accuracy of DFT formation energies. *NPJ Comput. Mater.* **2015**, *1*, 15010. [[CrossRef](#)]
46. Jain, A.; Ong, S.P.; Hautier, G.; Chen, W.; Richards, W.D.; Dacek, S.; Cholia, S.; Gunter, D.; Skinner, D.; Ceder, G.; et al. The Materials Project: A materials genome approach to accelerating materials innovation. *APL Mater.* **2013**, *1*, 011002. [[CrossRef](#)]
47. Gossett, E.; Toher, C.; Oses, C.; Isayev, O.; Legrain, F.; Rose, F.; Zurek, E.; Carrete, J.; Mingo, N.; Tropsha, A.; et al. AFLOW-ML: A RESTful API for machine-learning predictions of materials properties. *Comput. Mater. Sci.* **2017**, *152*, 134–145. [[CrossRef](#)]
48. Feufel, H.; Schuller, F.; Schmid, J.; Sommer, F. Calorimetric study of ternary liquid Al-La-Ni alloys. *J. Alloy. Compd.* **1997**, *257*, 234–244. [[CrossRef](#)]
49. Sommer, F.; Schmid, J.; Schuller, F. Temperature and concentration dependence of the enthalpy of formation of liquid Al-La-Ni Alloys. *J. Non-Cryst. Solids* **1996**, *205*, 352–356. [[CrossRef](#)]
50. Schmid, J.; Sommer, F. Heat Capacity of Liquid Al-La-Ni Alloys. *Thermochim. Acta* **1998**, *314*, 111–121. [[CrossRef](#)]
51. Pasturel, A.; Chatillon-Colinet, C.; Guegan, A.P. Thermodynamic properties of $LaNi_4M$ compounds and their related hydrides. *J. Less-Common Met.* **1982**, *84*, 73–78. [[CrossRef](#)]
52. Borzone, G.; Raggio, R.; Delsante, S. Chemical and thermodynamic properties of several Al-Ni-R systems. *Intermetallics* **2003**, *11*, 1217–1222. [[CrossRef](#)]
53. Cheary, R.W.; Coelho, A.A. Fundamental parameters approach to X-ray line-profile fitting. *J. Appl. Crystallogr.* **2010**, *25*, 109–121. [[CrossRef](#)]
54. Coelho, A.A. Indexing of powder diffraction patterns by iterative use of singular value decomposition. *J. Appl. Crystallogr.* **2003**, *36*, 86–95. [[CrossRef](#)]
55. Cao, W.; Chen, S.L.; Zhang, F.; Wu, K.; Yang, Y.; Chang, Y.A. Pandat Software with PanEngine, PanOptimizer and PanPrecipitation for Multi-component Phase Diagram Calculation and Materials Property Simulation. *Calphad* **2009**, *33*, 328–342. [[CrossRef](#)]
56. Dinsdale, A.T. SGTE data for pure elements. *Calphad* **1991**, *15*, 317–425. [[CrossRef](#)]



© 2018 by the authors. Licensee MDPI, Basel, Switzerland. This article is an open access article distributed under the terms and conditions of the Creative Commons Attribution (CC BY) license (<http://creativecommons.org/licenses/by/4.0/>).